Model Reference Adaptive Control for Aortic Pressure Regulation in *Ex Vivo* Heart Perfusion

Liming Xin, Weiran Yao, Yan Peng, Naiming Qi, Shaorong Xie, Changhai Ru, Mitesh Badiwala, and Yu Sun, *Fellow, IEEE*

***Abstract*— This brief proposes the first model reference adaptive control (MRAC) method for aortic pressure (AoP) regulation and maintaining the heart's physiological aerobic metabolism in *ex vivo* heart perfusion (EVHP). A mathematical model of the EVHP was established to describe the hemodynamic behavior of EVHP and quantify the changes in cardiac parameters. A reference model consisting of a virtual proportional–integral–derivative (PID) controller and the EVHP model was employed to generate the reference trajectory of AoP. An adaptation algorithm tunes the control parameters based on the reference model and the isolated heart. Experiments were conducted using large animal hearts (50 ± 5 kg porcine) to validate the adaptive controller's performance for stepwise and fast switching AoP references. The results confirmed the effectiveness of the proposed controller for regulating the AoP in isolated porcine hearts, in an accurate (mean error less than 2 mmHg) and fast (4–8 s of settling time) manner.**

***Index Terms*— Automated organ perfusion, closed-loop control, *Ex vivo* heart, model reference adaptive control (MRAC).**

I. Introduction

THE *Ex vivo* perfusion of an isolated heart with oxygenated and nutrient-enriched perfusate is critical for heart transplantation [1]–[3]. In *ex vivo* heart perfusion (EVHP), aortic pressure (AoP) regulation plays an important role in maintaining the heart's physiological aerobic metabolism. In current EVHP, AoP is manually regulated based on trial and error [4], [5]. Delays and large fluctuations (e.g., overshoot >5% of mean AoP) in AoP regulation affect heart's normal metabolism and cause irregular heartbeat and organ damage [6]. Ideally, AoP regulation should be performed by a closed-loop controller built with exact knowledge of isolated hearts. However, an important challenge faced during EVHP controller development is that cardiac parameters vary significantly during perfusion and across different hearts. For instance, hearts are rewarmed from 4 °C to 37.6 °C in perfusion; with the increasing heart temperature, the coronary vascular resistance drops rapidly (>50% reduction) [7]. The changes in cardiac parameters pose challenges to achieve smooth and fast transient response in AoP regulation.

Closed-loop blood pressure controllers for other organ perfusion systems (e.g., kidney and liver perfusion systems) based on model-free methods have been developed, in which proportional–integral–derivative (PID) is the main control method. For instance, Plaats [8] developed a PID controller to keep the perfusion pressure at a preset level in *ex vivo* liver perfusion. Post *et al.* [9] implemented a PID controller in an *ex vivo* kidney perfusion system for pressure regulation. Campos-Delgado *et al.* [10] proposed a PD controller to maintain a desired renal perfusion pressure. For these PID controllers, gain selection was not intuitive and required gain scheduling had to be appropriately tuned for different organs. Kornuta and Dixon [11] developed a linear explicit model predictive controller for *ex vivo* Lymphatic vessel perfusion. However, their identification model and model predictive control law are purely linear, and the predictive capabilities and dynamic control performance of the system are limited due to the inherent nonlinear behavior of isolated organs.

Despite the previous efforts in developing blood pressure regulation technologies for organ perfusion, the development of an AoP control system with satisfactory transient performance for isolated hearts has not been achieved due to the changes in cardiac parameters. To tackle the parameter-varying plant, one feasible approach is to estimate these varying parameters and adjust the controller based on the estimation results [12]. However, the complexity of the EVHP process makes it difficult to find an explicit relationship between the parameters of the plant and the controller performance.

This brief presents a model reference adaptive control (MRAC) method for regulating AoP in EVHP.

Manuscript received June 10, 2019; revised January 2, 2020; accepted February 24, 2020. Manuscript received in final form February 29, 2020. Recommended by Associate Editor J. B. Hoagg. *(Corresponding authors: Weiran Yao; Yan Peng; Yu Sun.)*

Liming Xin is with the Department of Mechanical and Industrial Engineering, University of Toronto, Toronto, ON M5S 3G8, Canada (e-mail: xin_liming@hotmail.com).

Weiran Yao and Naiming Qi are with the School of Astronautics, Harbin Institute of Technology, Harbin 150001, China (e-mail: yaoweiran@hit.edu.cn; qinm@hit.edu.cn).

Yan Peng is with the School of Mechatronic Engineering and Automation, Shanghai University, Shanghai 200444, China (e-mail: pengyan@shu.edu.cn).

Shaorong Xie is with the School of Computer Engineering and Science, Shanghai University, Shanghai 200444, China (e-mail: srxie@shu.edu.cn).

Changhai Ru is with the Research Center of Robotics and Micro System, Soochow University, Suzhou 215021, China, and also with the Jiangsu Provincial Key Laboratory of Advanced Robotics, Soochow University, Suzhou 215021, China (e-mail: rzh@suda.edu.cn).

Mitesh Badiwala is with the Faculty of Medicine, University of Toronto, Toronto, ON M5S 1A8, Canada, and also with the Department of Cardiovascular Surgery, University Health Network, Toronto, ON M5G 2N2, Canada (e-mail: mitesh.badiwala@uhn.ca).

Yu Sun is with the Department of Mechanical and Industrial Engineering, University of Toronto, Toronto, ON M5S 3G8, Canada, and also with the Department of Electrical and Computer Engineering, University of Toronto, Toronto, ON M5S 3G8, Canada (e-mail: sun@mie.utoronto.ca).

This article has supplementary downloadable material available at http://ieeexplore.ieee.org, provided by the authors.

Color versions of one or more of the figures in this article are available online at http://ieeexplore.ieee.org.

Digital Object Identifier 10.1109/TCST.2020.2978448

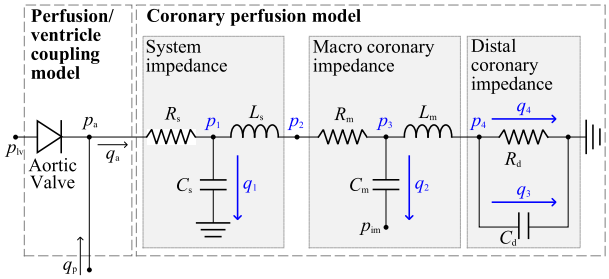

Fig. 1. Electrical analog of EVHP model.

In literatures, MRAC has been employed to handle model complexity and disturbance in applications such as rotor control [13], [14], bending actuators control [15], [16], and voltage/current control [17]–[19]. The contributions of this brief are as follows.

1) A mathematical model is established to describe the hemodynamic behavior of EVHP and quantify the changes in cardiac parameters.
2) The EVHP model combined with a virtual PID controller forms a closed-loop reference model. Virtual PID gains are tuned based on the updated cardiac parameters to generate the reference trajectory of AoP.
3) An adaptive algorithm is designed to adapt to the cardiac changes and achieve AoP regulation rapidly and smoothly.

Experiments were conducted using large animal hearts (50 ± 5 kg, 6 pig hearts). The results show that the proposed MRAC is capable of regulating the AoPs of isolated pig hearts in an accurate (mean error less than 2 mmHg) and fast (4–8 s of settling time) manner.

II. Modeling of EVHP

This section describes the mathematical modeling and hemodynamic characteristics of the EVHP system. Previous studies suggest that EVHP can be elucidated by a coronary circulation model [20]. However, such a model does not account for the effect of left ventricular pressure on AoP through the aortic valve when the left ventricle is primed with perfusate in EVHP. Therefore, in our model, a coronary circulation model is integrated with the perfusion/ventricle coupling model (Fig. 1). Table I lists the state variables of EVHP, and Table II lists cardiac parameters that change over time and across different hearts.

Flow inertia (L_m and L_s) and compliance (C_d) of the distal vessels are integrated with the coronary model to better reflect the effect of coronary pressure fluctuations on AoP compared to previous models in [20] and [21]. According to Kirchhoff laws, the system impedance is

$$p_a - p_1 = R_s q_a \tag{1}$$

$$C_s \frac{dp_1}{dt} = q_1 \tag{2}$$

$$p_1 - p_2 = L_s \left(\frac{dq_2}{dt} + \frac{dq_3}{dt} + \frac{dq_4}{dt} \right). \tag{3}$$

TABLE I
State Variables of EVHP

State variables	Unit	Physiological meaning
p_a	mmHg	AoP
q_a	ml s^{-1}	Aortic flow
MAP	mmHg	Mean AoP (MAP)
p_1	mmHg	Blood pressure behind R_s
p_2	mmHg	Blood pressure behind L_s
p_3	mmHg	Blood pressure behind R_m
q_1	ml s^{-1}	Blood flow through C_s
q_2	ml s^{-1}	Blood flow through C_m
q_3	ml s^{-1}	Blood flow through R_d
q_4	ml s^{-1}	Blood flow through C_d

TABLE II
Cardiac Parameters of EVHP

Cardiac parameters	Unit	Physiological meaning
R_s	mmHg·s/mL	System resistance
C_s	mL/mmHg	Aortic compliance
L_s	mmHg·s^2/mL	System flow inertia
R_m	mmHg·s/mL	Macro coronary resistance
C_m	mL/mmHg	Macro coronary compliance
L_m	mmHg·s^2/mL	Flow inertia in macro coronary
R_d	mmHg·s/mL	Distal coronary resistance
C_d	mL/mmHg	Distal coronary compliance

The macro coronary impedance is

$$p_2 - p_3 = R_m (q_2 + q_3 + q_4) \tag{4}$$

$$C_m \left(\frac{dp_3}{dt} - \frac{dp_{\text{im}}}{dt} \right) = q_2 \tag{5}$$

$$p_3 - p_4 = L_m \left(\frac{dq_3}{dt} + \frac{dq_4}{dt} \right) \tag{6}$$

where p_{im} is the intramyocardial pressure. Distal coronary impedance is

$$p_4 = R_d q_3 \tag{7}$$

$$C_d \frac{dp_4}{dt} = q_4. \tag{8}$$

Aortic flow q_a is the sum of q_1, q_2, q_3, and q_4 i.e., $q_a = q_1 + q_2 + q_3 + q_4$. Clinically, MAP is calculated by

$$\text{MAP} = \int_{t_0}^{t_1} \frac{p_a}{T} dt \approx \frac{1}{3}\overline{p_a(t)} + \frac{2}{3}\underline{p_a(t)} \tag{9}$$

where t_0 is the start time of the cardiac cycle, t_1 is the end time of the cardiac cycle. $T = t_1 - t_0$ is the cardiac cycle time. $\underline{p_a(t)} = \min(p_a)$ and $\overline{p_a(t)} = \max(p_a)$ during each cycle T.

In diastole, the muscle of the heart is relaxed and the left ventricular pressure p_{lv} is much lower than the AoP generated by the perfusion flow q_p. The diode is open-circuited and $q_a = q_p$ during this period. Thus, the hemodynamic behavior of the model is determined by q_p and p_{im}. Equation (1) becomes

$$p_a - p_1 = R_s q_p. \tag{10}$$

In systole, the heart contracts, and p_{lv} generated by the heart contraction is higher than the AoP generated by the perfusion flow q_p. The diode is short-circuited and $p_a = p_{\mathrm{lv}} - p_c$ during this period, where p_{lv} is the left ventricular pressure and p_c is a constant pressure drop [22]. The aortic flow q_a equals the sum of the perfusion flow q_p and the blood flow generated by the left ventricle contraction in systole. The hemodynamic behavior of the model is determined by p_{lv}. Equation (1) becomes

$$p_{\mathrm{lv}} - p_c - p_1 = R_s q_a. \tag{11}$$

The state equation for the EVHP model is

$$\begin{bmatrix} \dfrac{d\boldsymbol{x}(t)}{dt} & y(t) \end{bmatrix}^{\mathrm{T}} = \begin{bmatrix} \boldsymbol{A}(t) & \boldsymbol{B}(t) \\ \boldsymbol{C} & 0 \end{bmatrix} \begin{bmatrix} \boldsymbol{x}(t) \\ u(t) \end{bmatrix} + \boldsymbol{X}(t)\,\boldsymbol{\delta}(t) \tag{12}$$

where state vector $\boldsymbol{x}(t)$, disturbances $\boldsymbol{\delta}(t)$, control variable $u(t)$, and output variable $y(t)$ are

$$\begin{aligned} \boldsymbol{x}(t) &= \begin{bmatrix} \mathrm{MAP} & p_1 & p_2 & p_3 & p_4 & q_1 & q_2 & q_3 & q_4 \end{bmatrix}^{\mathrm{T}} \\ \boldsymbol{\delta}(t) &= \begin{bmatrix} \delta_1(t) & \delta_2(t) \end{bmatrix}^{\mathrm{T}} = \begin{bmatrix} \frac{dp_{\mathrm{lv}}}{dt} & \frac{dp_{\mathrm{im}}}{dt} \end{bmatrix}^{\mathrm{T}} \\ u(t) &= \frac{dq_p}{dt}, \qquad y(t) = \mathrm{MAP}. \end{aligned} \tag{13}$$

$\delta_1(t)$ and $\delta_2(t)$ are determined by the heart (e.g., heart contractility, heart rate and heart size), which cannot be predicted. $u(t)$ can be directly controlled by the perfusion system. From (2)–(9), the state matrix $\boldsymbol{A}(t)$, control matrix $\boldsymbol{B}(t)$, output matrix $\boldsymbol{C}$, and disturbance matrix $\boldsymbol{X}(t)$ are described as

$$\boldsymbol{A}(t) = \begin{bmatrix} 0 & \frac{1}{T} & 0 & 0 & 0 & \frac{R_s}{T} & \frac{R_s}{T} & \frac{R_s}{T} & \frac{R_s}{T} \\ 0 & 0 & 0 & 0 & 0 & \frac{1}{C_s} & 0 & 0 & 0 \\ 0 & \frac{R_m}{L_s} & \frac{-R_m}{L_s} & 0 & 0 & 0 & \frac{1}{C_m} & 0 & 0 \\ 0 & 0 & 0 & 0 & 0 & 0 & \frac{1}{C_m} & 0 & 0 \\ 0 & 0 & 0 & 0 & 0 & 0 & 0 & \frac{1}{C_d} & 0 \\ 0 & \frac{-1}{L_s} & \frac{1}{L_s} & 0 & 0 & \frac{-J(t)}{R_s C_s} & 0 & 0 & 0 \\ 0 & \frac{1}{L_s} & \frac{-1}{L_s} & \frac{-1}{L_d} & \frac{1}{L_d} & 0 & 0 & 0 & 0 \\ 0 & 0 & 0 & \frac{1}{L_d} & \frac{-1}{L_d} & 0 & 0 & \frac{-1}{R_d C_d} & 0 \\ 0 & 0 & 0 & 0 & 0 & 0 & 0 & \frac{1}{R_d C_d} & 0 \end{bmatrix}$$

$$\boldsymbol{B}(t) = \begin{bmatrix} 0 & 0 & 0 & 0 & 0 & 1 & -J(t) & 0 & 0 & 0 \end{bmatrix}^{\mathrm{T}}$$

$$\boldsymbol{C} = \begin{bmatrix} 1 & 0 & 0 & 0 & 0 & 0 & 0 & 0 & 0 \end{bmatrix}$$

$$\boldsymbol{X}(t) = \begin{bmatrix} 0 & 0 & 0 & 0 & 0 & \frac{J(t)}{R_s} & 0 & 0 & 0 & 0 \\ 0 & 0 & 1 & 1 & 0 & 0 & 0 & 0 & 0 & 0 \end{bmatrix}^{\mathrm{T}}. \tag{14}$$

The indicator function $J(t)$ is introduced because the hemodynamic model of the EVHP is different in diastole and systole. Here, $J(t)$ describes the short-circuit and open-circuit behavior of the diode

$$J(t) = \begin{cases} 1, & \text{systole} \\ 0, & \text{diastole.} \end{cases} \tag{15}$$

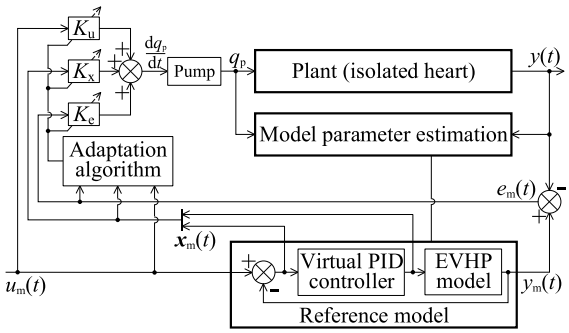

Fig. 2. Block diagram of the adaptive control system.

III. Controller Design

To tackle the uncertain and time-varying cardiac parameters, we developed an MRAC method for AoP regulation in EVHP. Fig. 2 depicts the block diagram of the proposed adaptive control system. The target MAP [denoted as $u_m(t)$] and measured MAP [denoted as $y(t)$] are the input and output of the system, respectively. A reference model comprising a virtual PID controller and a mathematical model of EVHP is established to produce reference trajectories of MAP. Cardiac parameters and the virtual controller gains are updated in real time to make the model always adapting to the changes in the plant. By tracking the reference trajectory, an adaptive algorithm realizes optimized AoP control. The difference between target MAP and measured MAP is used as feedback to tune the control gains to compensate for the dynamic error in AoP regulation.

A. Cardiac Parameter Estimation

The time-varying cardiac parameters are estimated as

$$S^* = \arg\min_{S} \left(\mathrm{RMSE}\left(p_{a,t_0 \to t_1}, \widehat{p_{a,t_0 \to t_1}} \right) \right) \tag{16}$$

where RMSE is the root-mean-square error method, $p_{a,t_0 \to t_1}$ is the trajectory of measured AoP from t_0 to t_1, and $\widehat{p_{a,t_0 \to t_1}}$ is the prediction of AoP trajectory, which is predicted by our perfusion model. $S = \{R_s\ C_s\ L_s\ R_m\ C_m\ L_m\ R_d\ C_d\}$ represents the cardiac parameter configuration. Using the measured flow rate as input to the EVHP model, we fit the predicted AoP waveform to the measured AoP waveform by adjusting the cardiac parameters in the physiological range. The estimation of cardiac parameters is performed via "trial-and-error." A few iterations in practice suffice. The values of the cardiac parameters that minimize the difference between $\widehat{p_{a,t_0 \to t_1}}$ and $p_{a,t_0 \to t_1}$ i.e., RMSE of the AoP waveform are the best estimate of S^* [12], [25].

B. Reference Model

The objective of the adaptive control system is to adapt to the heart uncertainty so as to track the reference MAP trajectory in a smooth and rapid manner. Typically, a reference model is formulated as a linear time-invariant system [26]. However, an isolated heart is a nonlinear time-variant system, which increases the complexity in reference MAP trajectory

generation. To overcome this difficulty, a reference model consisting of a virtual PID controller and the proposed EVHP model is employed to generate a reference MAP trajectory (see Fig. 2). The reference model is represented by the following function:

$$\left[\frac{d\boldsymbol{x}_m(t)}{dt}\ y_m(t)\right]^{\mathrm{T}} = F\left(\boldsymbol{A}(t), \boldsymbol{B}(t), \boldsymbol{C}, \boldsymbol{X}, \boldsymbol{x}_m(t), u_m(t)\right). \tag{17}$$

Since describing the function F by explicit state matrices is difficult, numerical methods are used to solve the differential equation (17). The state variables $\boldsymbol{x}_m(t)$, reference model input $u_m(t)$, and output $y_m(t)$ are chosen as

$$\boldsymbol{x}_m(t) = [x_{m1}(t)\ \ x_{m2}(t)]^{\mathrm{T}}, \quad u_m(t) = \mathrm{MAP}^*, \ \ y_m(t) = \mathrm{MAP} \tag{18}$$

where $x_{m1}(t)$ is the deviation between $u_m(t)$ and $y_m(t)$, $x_{m2}(t)$ is the acceleration of perfusion flow rate generated by the virtual PID controller, and MAP* is the target value of MAP.

The matrices $\boldsymbol{A}$, $\boldsymbol{B}$, $\boldsymbol{C}$, and $\boldsymbol{X}$ are derived by cardiac parameters [estimated by (16)] and virtual PID control gains. Virtual PID gains are calculated by the following procedures.

1) Construct closed-loop control of $y_m(t)$ with an arbitrary proportional control K_{VP}. Generate trajectory of $y_m(t)$ via numerical method (Runge–Kutta method)

$$\begin{aligned}\widetilde{y_m}(t) &= \widehat{p_{a,t_0\to t_1}} \\ &= \mathcal{N}(\mathrm{S}(\boldsymbol{A},\boldsymbol{B},\boldsymbol{C},\boldsymbol{X}), K_{\mathrm{VP}}, \boldsymbol{t}_{t_0\to t_1}, \boldsymbol{x}_m(0), \boldsymbol{u}_{t_0\to t_1}).\end{aligned} \tag{19}$$

2) Calculate the virtual PID control gains K^*_{VP}, K^*_{VI} and K^*_{VD} based on $\widetilde{y_m}(t)$ using Ziegler–Nichols rule [27].

In (19), $\mathcal{N}(\cdot)$ is the numerical solution based on Runge-Kutta method, $S(\boldsymbol{A},\boldsymbol{B},\boldsymbol{C},\boldsymbol{X})$ represents the reference model system based on (17), $\boldsymbol{t}_{t_0\to t_1}$ is the time series from t_0 to t_1, $\boldsymbol{x}_m(0)$ is the initial states of the reference model system, and $\boldsymbol{u}_{t_0\to t_1}$ is the series of control input which corresponds to $u_m(t)$, $t \in [t_0, t_1]$.

When the virtual PID gains are determined, the reference trajectory $y_m(t)$ will be generated by a numerical method based on the estimated cardiac parameters and the virtual PID control gains

$$\begin{aligned}y_m(t) &= \widehat{p_{a,t_0\to t_1}} \\ &= \mathcal{N}\left(S(\boldsymbol{A},\boldsymbol{B},\boldsymbol{C},\boldsymbol{X}), \left[K^*_{\mathrm{VP}}, K^*_{\mathrm{VI}}, K^*_{\mathrm{VD}}\right]\right. \\ &\quad \left.\boldsymbol{t}_{t_0\to t_1}, \boldsymbol{x}_m(0), \boldsymbol{u}_{t_0\to t_1}\right).\end{aligned} \tag{20}$$

C. Adaptive Controller

This section describes a control law to calculate the control command of the adaptive controller. An adaptive algorithm is designed to refine the transient performance of the controller.

1) Control Law: Let $\boldsymbol{x}^*(t)$ and $\boldsymbol{u}^*(t)$ be the ideal trajectories of $\boldsymbol{x}(t)$ and $\boldsymbol{u}(t)$, respectively. Then

$$\begin{bmatrix}\dfrac{d\boldsymbol{x}^*(t)}{dt} \\ y^*(t)\end{bmatrix} = \begin{bmatrix}\boldsymbol{A}(t) & \boldsymbol{B}(t) \\ \boldsymbol{C}(t) & 0\end{bmatrix}\begin{bmatrix}\boldsymbol{x}^*(t) \\ \boldsymbol{u}^*(t)\end{bmatrix} \tag{21}$$

where $y^*(t) = y_m(t)$. For the reference model, a linear mapping relationship between $[\boldsymbol{x}^*(t)\ \boldsymbol{u}^*(t)]^{\mathrm{T}}$ and $[\boldsymbol{x}_m(t)\ u_m(t)]^{\mathrm{T}}$ exists [28]–[30]

$$\begin{bmatrix}\boldsymbol{x}^*(t) \\ \boldsymbol{u}^*(t)\end{bmatrix} = \begin{bmatrix}A_{11} & A_{12} \\ A_{21} & A_{22}\end{bmatrix}\begin{bmatrix}\boldsymbol{x}_m(t) \\ u_m(t)\end{bmatrix} \tag{22}$$

where A_{11}, A_{12}, A_{21}, and A_{22} are constant matrices. Thus, a feasible adaptive control law has the following form:

$$\begin{aligned}u = \frac{dq_p}{dt} &= K_e\left(y_m(t) - y(t)\right) + \boldsymbol{u}^*(t) \\ &= K_e e_m(t) + A_{21}\boldsymbol{x}_m(t) + A_{22}u_m(t)\end{aligned} \tag{23}$$

where K_e is the adaptive gain for the output deviation and $e_m(t) = y_m(t) - y(t)$. Explicit forms of matrices A_{21} and A_{22} cannot be obtained because (22) is underdetermined. As a solution, we employ an alternative controller where the matrices A_{21} and A_{22} in (23) are substituted with adaptive gains K_x and K_m. When the control command exceeds the upper or lower bound of the system input, the pump input becomes saturated. For this, a correction term S_{SAT} is introduced into the control law to avoid saturation

$$\begin{aligned}u &= [K_e\ K_x\ K_m][e_m(t)\ \ \boldsymbol{x}_m(t)\ \ u_m(t)]^{\mathrm{T}} - S_{\mathrm{SAT}} \\ &= [K_1\ K_2\ K_3\ K_4][e_m(t)\ \ x_{m1}(t)\ \ x_{m2}(t)\ \ u_m(t)]^{\mathrm{T}} - S_{\mathrm{SAT}}\end{aligned} \tag{24}$$

where $K_e = K_1$, $K_x = [K_2\ K_3]$, and $K_m = K_4$ are the adaptive control gains for the reference model states and input.

The correction term S_{SAT} is updated by PI control to eliminate the portion of the control input that exceeds the upper and lower limits, that is

$$S_{\mathrm{SAT}} = K_{s1}\left[u(t) - \mathrm{SAT}(u(t))\right] + K_{s2}\int_{t_0}^{t_1}\left[u(t) - \mathrm{SAT}(u(t))\right]dt \tag{25}$$

where K_{s1} and K_{s2} are coefficients. SAT$(\cdot)$ represents the saturation function

$$\mathrm{SAT}(u(t)) = \begin{cases}u_{\min}, & u(t) \le u_{\min} \\ u(t), & u_{\min} \le u(t) \le u_{\max} \\ u_{\max}, & u_{\max} \le u(t)\end{cases} \tag{26}$$

where $u_{\min}$ and $u_{\max}$ are the lower and upper bounds, respectively, of the control variable $u(t)$. When $u(t)$ is out of range, the correction term S_{SAT} is generated through PI control to secure $u(t)$ in the normal range (between $u_{\min}$ and $u_{\max}$). The integral and proportional terms are used to make the saturation correction change smoothly [28], [32].

2) Adaptive Algorithm: The adaptive algorithm calculates the control gains K_u, K_x, and K_e in the control law shown in (24) and guarantees the transient performance of the control system. The calculation of these gains involves the information of the plant output $y(t)$ and the control target $u_m(t)$, which can guarantee the convergence to the control reference $y_m(t)$. In addition, the input and output of the virtual PID controller in the reference model are used to feedback transient errors of reference $y_m(t)$ (delay and overshoot) caused by the virtual PID controller. The adaptation algorithm is

$$\begin{cases} K_1 = K_{1\mathrm{I}} \left(\int_{t_0}^{t_1} e_m^2(t)\, dt \right) + K_{1\mathrm{P}} e_m^2(t) \\ K_2 = K_{2\mathrm{P}} e_m(t) / |e_m(t)| \\ K_3 = K_{3\mathrm{P}} e_m(t) / |e_m(t)| \\ K_4 = K_{4\mathrm{I}} \left(\int_{t_0}^{t_1} e_m(t)\, u_m(t)\, dt \right) + K_{4\mathrm{P}} e_m(t)\, u_m(t) \end{cases} \tag{27}$$

where $K_{1\mathrm{I}}$, $K_{4\mathrm{I}}$, $K_{1\mathrm{P}}$, $K_{2\mathrm{P}}$, $K_{3\mathrm{P}}$, and $K_{4\mathrm{P}}$ are positive coefficients. In order to achieve a smooth AoP regulation, both the integral and proportional terms are used in the adaptive algorithm [28], [31]. K_1 and K_2 are the gains for $e_m(t)$ and $x_{m1}(t)$, respectively. They are positively correlated with $e_m(t)$ to ensure that $K_1 e_m(t)$ and $K_2 x_{m1}(t)$ are always the negative feedback for the error between the control reference $y_m(t)$ and the plant output $y(t)$ and the error between the control target $u_m(t)$ and the plant output $y(t)$, respectively. K_3 is the gain for $x_{m2}(t)$, determined by $e_m(t)$ and $x_{m2}(t)$. Thus, the corresponding term $K_3 x_{m2}(t)$ can be guaranteed a negative feedback of $e_m(t)$, and its absolute value is regulated by $x_{m2}(t)$. K_4 for $u_m(t)$ is calculated in the same way as K_3.

Based on the adaptive algorithm in (27), control law (24) adapts to the changes in plant parameters. Thus, the control input (aortic flow rate acceleration) generated by the control law achieves fast and smooth AoP regulation.

D. Stability Analysis

The stability of the proposed MRAC is analyzed using the Lyapunov function. In our system, the variables $x_{m1}(t)$ is the deviation between the target MAP [denoted as $u_m(t)$] and the model output $y_m(t)$. $x_{m1}(t)$ represents the control of MAP by the virtual controller in the reference model. $e_m(t)$ is the deviation between the real MAP [denoted as $y(t)$] and the model output ym(t). $e_m(t)$ represents the tracking of the reference model by the adaptive controller. Both the virtual controller and the tracking control of the reference model will influence the effectiveness of the MRAC. Therefore, the Lyapunov function is established as a function of these two variables. A quadratic function is built as the system's Lyapunov function, which is positive definite in the variables $x_{m1}(t)$ and $e_m(t)$

$$V(t) = \frac{1}{2} e_m(t)^2 + \frac{1}{2} x_{m1}(t)^2 . \tag{28}$$

Target MAP $u_m(t)$ is invariant over time. The time derivative of the Lyapunov function is then

$$\begin{aligned} \frac{dV(t)}{dt} &= e_m(t) \frac{de_m(t)}{dt} + x_{m1}(t) \frac{dx_{m1}(t)}{dt} \\ &= e_m(t) \left(\frac{dy_m(t)}{dt} - \frac{dy(t)}{dt} \right) + x_{m1}(t) \frac{dy_m(t)}{dt}. \end{aligned} \tag{29}$$

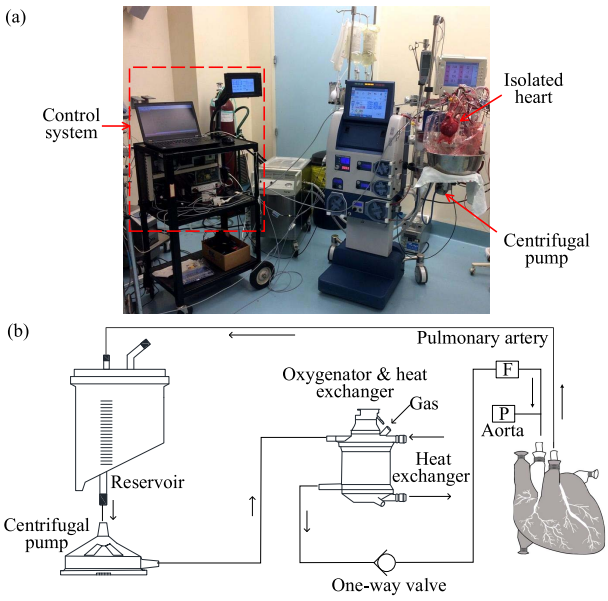

Fig. 3. (a) EVHP system for experiments. (b) EVHP diagram. P is the pressure sensor measuring the AoP, and F is the flow probe measuring the aortic flow.

Under physiological conditions, $\overline{p_a(t)}$ and $\underline{p_a(t)}$ can be described as $\overline{p_a} = a\underline{p_a(t)}$ where a is a positive constant, and $[(d\underline{p_a(t)})/dt]$ is proportional to (dq_p/dt) [22]–[24]. The calculation of MAP according to (9) gives

$$\frac{dy}{dt} \approx \frac{1}{3} \frac{d\overline{p_a(t)}}{dt} + \frac{2}{3} \frac{d\underline{p_a(t)}}{dt} \approx \left(\frac{1}{3} a + \frac{2}{3} \right) \frac{d\underline{p_a(t)}}{dt} \approx ku \tag{30}$$

where k is a positive constant. As the EVHP model mimics the hemodynamic characteristics of the isolated heart, the following function analogously holds:

$$\frac{dy_m}{dt} \approx k x_{m2}(t) . \tag{31}$$

Equations (30) and (31) give

$$\begin{aligned} \frac{dV(t)}{dt} &= e_m(t) \left(\frac{dy_m(t)}{dt} - \frac{dy(t)}{dt} \right) + k x_{m1}(t)\, x_{m2}(t) \\ &= k e_m(t) (x_{m2} - u) + k x_{m1}(t)\, x_{m2}(t) . \end{aligned} \tag{32}$$

According to the control law (24) and the adaptation algorithm (27), if we set $K_{3\mathrm{P}} > 1$, then $k e_m(t)(x_{m2} - u)$ is negative definite. Meanwhile, the virtual PID controller guarantees $k x_{m1}(t) x_{m2}(t)$ to be negative definite. Therefore, $y = u_m$ is globally asymptotically stable.

IV. Results

Simulations and animal experiments were performed. Male Yorkshire pig (55 ± 5 kg) hearts were used in the experiments. All animals received humane care in accordance with the Canadian Council on Animal Care guidelines. Institutional Animal Care Committee of the University Health Network approved all animal protocols.

The experimental system is shown in Fig. 3. The adaptive controller for regulating AoP was implemented on a PLC (FX5U, Mitsubishi, Japan), and parameter estimation was

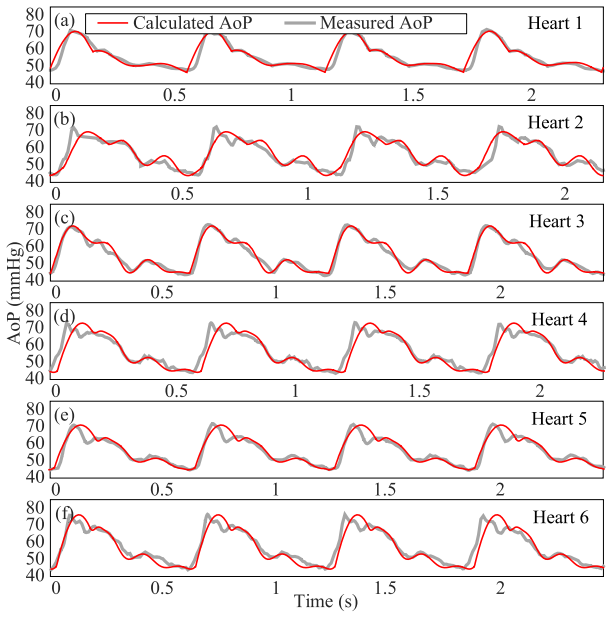

Fig. 4. Experimentally measured and model-calculated AoP. (a)–(f) AoP waveforms of heart 1 to heart 6 obtained from the model and experiments, respectively.

conducted iteratively every five minutes with a PC connected to the PLC. The perfusate flows from the reservoir to the centrifugal pump, and then to the oxygenator which exposes the perfusate to oxygen. Oxygenated perfusate was emptied into the coronary sinus over the aorta to maintain the myocardial aerobic metabolism and then into the right ventricle where it was ejected back to the reservoir through the pulmonary artery. AoP and aortic flow rate were measured at the inflow of the aorta with the sampling rate of 50 Hz.

A. Model Validation

Model validation was conducted by comparing the AoP waveforms estimated from the model [see (1)–(15)] with experimentally measured AoP waveforms. Six pig hearts were used in EVHP experiments for model validation. AoP and aortic flow rate were recorded during the experiments. In each experiment, two sets of AoP and aortic flow rate data were measured within 10 minutes with perfusion temperature kept constant to ensure that the changes of cardiac parameters be negligible during the measurement period. Cardiac parameters of each heart were estimated by (16) using the first set of AoP and aortic flow data measured in the experiment. The second set of aortic flow data was fed into the model (Fig. 1) with the estimated cardiac parameters to calculated the AoP waveform. The calculated AoP was compared to the measured AoP of the second set. Fig. 4 shows AoP waveforms obtained from the model and experiments. In all hearts, close agreement was found, and the errors between the model-predicted AoP and experimentally measured AoP are less than 5% (Table III), proving that our model is capable of accurately describing the hemodynamic behavior of EVHP.

B. Simulation Results

1) Simulation 1 (Changing Cardiac Parameters): Simulations were performed to assess the system's control performance under different cardiac parameters (Table IV). We repeated the simulation with parameters (shown in Table IV) that were obtained from two hearts in EVHP experiments. A step signal of 30–60 mmHg was used as input to test the system's adaptability. The proposed adaptive method was compared with a traditional PID controller in this simulation. PID control gains for achieving the shortest settling time without overshoot were obtained based on the cardiac parameters of heart 1.

TABLE III
RESULTS OF MODEL VALIDATION

Heart No.	1	2	3	4	5	6
Error	2.2%	3.7%	1.6%	4.2%	2.4%	3.1%

TABLE IV
CARDIAC PARAMETERS

Parameters	R_s	C_s	L_s	R_m	C_m	L_m	R_d	C_d
heart 1	0.6*	0.5	0.12	1.2	0.6	0.007	1.8	0.3
heart 2	0.7	0.42	0.15	1.1	0.4	0.01	2.2	0.24

* Units of the variables are given in Table II.

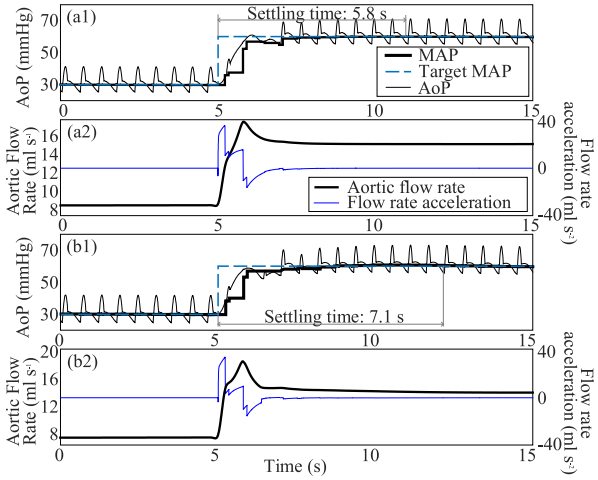

Fig. 5. Tracking response of MRAC controller. (a1) Tracking response of heart 1. (a2) Perfusion flow of heart 1. (b1) Tracking response of heart 2. (b2) Perfusion flow of heart 2.

Figs. 5 and 6 show the pressure tracking performance by the two control methods. To quantify the response speed of the two methods, the settling time of the system was measured with an error band of 2%. It can be observed that both control methods can achieve reference pressure tracking by regulating the pump speed; however, the adaptive control approach [Fig. 5(a1) and (b1)] resulted in shorter settling time than the PID controller [Fig. 6(a1) and (b1)]. The settling time was <7.5 s by MRAC versus <9 s by PID controller for tracking the step of 30 mmHg. In addition, compared to the traditional PID control method with constant control parameters, the proposed adaptive control method revealed smaller overshoot (less than 2 mmHg) in the two simulations [see Fig. 5(a1) and (b1)].

Since the PID control gains were tuned based on heart 1, AoP regulation of heart 1 by PID controller also

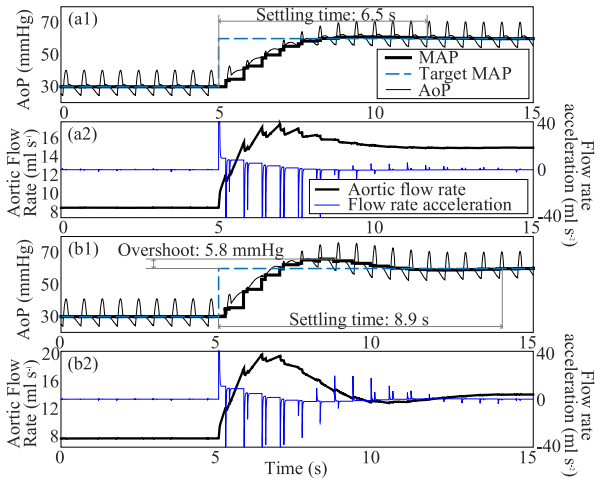

Fig. 6. Tracking response of PID controller. (a1) Tracking response of heart 1. (a2) Perfusion flow of heart 1. (b1) Tracking response of heart 2. (b2) Perfusion flow of heart 2.

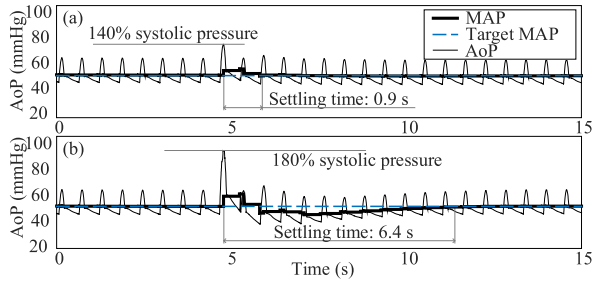

Fig. 7. Tracking response with (a) small pulse input (140% of normal systolic pressure) and (b) high pulse input (180% of normal systolic pressure).

achieved a short settling time (6.5 s) and small overshoot (less than 2 mmHg). When the AoP of heart 2 was regulated by the same PID control gains determined in the experiment of heart 1, overshoot increased from less than 2–5.8 mmHg, due to the fact that the blood vessel resistance of heart 2 was higher than that of heart 1 (Table IV). Although the performance of the PID controller can be improved by gain tuning for each individual hearts, control gain tuning must be avoided in EVHP. PID tuning is based on trial and error and brings irreversible cardiac injury (endothelial cell injury). Therefore, the proposed MRAC method is more adaptive across hearts and more suitable than PID control for EVHP.

The behaviors of the aortic flow rate and acceleration are shown in Figs. 5(a2) and (b2) and 6(a2) and (b2). There are more fluctuations in flow rate acceleration in PID control than in adaptive control. Aortic flow rate directly reflects the oxygen and nutrient supply which influences the cardiac metabolism. The large fluctuations in the flow rate and sharp changes in the flow rate acceleration during PID control causes red blood cell's damage myocardial injury. Smooth waveforms of flow rate and flow rate acceleration can prevent irregular heartbeats and cardiac injury (see Supplementary Video). In the proposed MRAC method, aortic flow rate acceleration is the pump control command (24) and is generated by (27). The control command is guaranteed smooth by using the integral terms of e_m in the adaptive algorithm. In contrast, the control gains of the PID controller are constant, making the control system too sensitive to e_m, u_m, and $\boldsymbol{x}_m$ at certain levels of e_m. Thus, the smoothness of generated control command cannot be guaranteed.

2) Simulation 2 (Irregular Heartbeat): In the proposed EVHP model [see (12)–(15)], disturbances $\boldsymbol{\delta}(t)$ is an uncontrollable input associated with heart contractility. Fluctuations of $\boldsymbol{\delta}(t)$ lead to irregular heartbeats which can cause disturbances to the AoP measurement. As AoP is the feedback, the controller's performance is affected by the measured AoP and thus also by δ_1. To assess the tolerance of the proposed controller to AoP disturbance, we performed simulations using two levels of irregular AoPs (140% of normal systolic pressure as commonly appeared in the experiments and 180% of normal systolic pressure as the upper limit of the irregular systolic pressure). In the simulation, $\delta_1 = 40\%$ systolic pressure and $\delta_1 = 80\%$ systolic pressure were fed into the model to mimic the irregular heartbeats in EVHP, respectively. Cardiac parameters (shown in Table IV) and aortic flow rate (as input) of heart 1 were used in this simulation. The simulation results shown in Fig. 7 indicate that the proposed MRAC controller is capable of tackling AoP disturbance in the perfusion process, while larger AoP disturbance causes a longer time for the system to reach the steady state.

C. Experimental Performance

Experiments were performed to investigate the performance of the proposed MRAC controller for achieving a desired MAP. Repeated experiments were performed using six pig hearts. The target MAP was varied in the range of 30 mmHg to 60 mmHg which is commonly used in EVHP in steps of 10 mmHg [1]–[3]. The first experiment was performed to assess the system's ability to achieve stepwise MAP setpoints. The changing rate of cardiac parameters was less than 5% during the AoP regulation period. Representative data from heart 3 shown in Fig. 8(a) confirmed that the proposed adaptive controller was capable of following the target MAP with an average settling time of 5–8 s, with almost zero overshoot and remaining stable over time. In the second experiment, the target MAP was first set at 40 mmHg and then raised to 60 mmHg. As shown in Fig. 8(b), the AoP transient performance did not reveal any overshoot, and the steady state was reached within 8 s. The response of the controller to a large switching reference (30 mmHg) was also tested, as shown in Fig. 8(c). The target MAP was changed from 30 to 60 mmHg. The control system again was able to follow the target MAP with almost zero overshoot.

For comparison, AoP regulation by a PID controller and an experienced operator of EVHP who followed a standard operation procedure were also conducted using six pig hearts at steps of 10 mmHg, 20 mmHg, and 30 mmHg. Fig. 9(a) and (b) shows the typical response in PID and manual control. They both resulted in apparent overshoot and irregular heartbeats, while the PID controller shows relatively faster response time. Large AoP overshoot and longer response time in manual control were caused due to the low manual AoP regulation

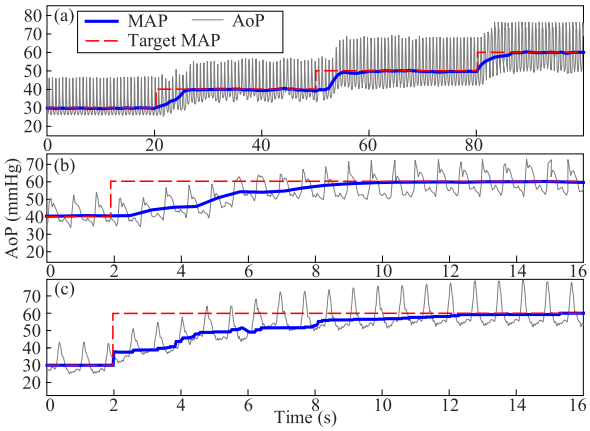

Fig. 8. Tracking response of the adaptive controller to desired MAP at step of (a) 10, (b) 20, and (c) 30 mmHg.

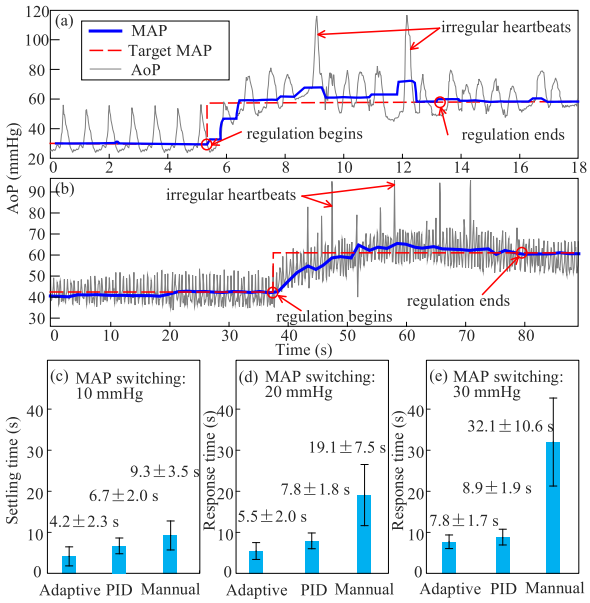

Fig. 9. (a) Representative manual control result of AoP. (b) Representative PID control result of AoP. (c)–(e) Statistics of the tracking results.

accuracy by tuning a mechanical knob, resulting in irregular heartbeats and even cardiac arrest. For tracking steps of 10, 20, and 30 mmHg, as shown in Fig. 9(c)–(e), the adaptive controller had significantly faster response without causing any irregular heartbeats (see Supplementary Video). With pressure changes of 10, 20, and 30 mmHg, the mean settling time of the adaptive controller was 4.2 ± 2.3, 5.5 ± 2.0, and 7.8 ± 1.7 s, while the settling time of PID control was 6.7 ± 2.0, 7.8 ± 1.8, and 8.9 ± 1.9 s, and the settling time of manual control was 9.3 ± 3.5, 19.1 ± 7.5, and 32.1 ± 10.6 s, respectively. At the same MAP changing step, manual regulation time varies widely due to the lack of knowledge in the change of cardiac parameters and empirical knob regulation.

V. Conclusion

This brief reported an MRAC method for the regulation of AoP in EVHP, which ensures the proper level of aerobic metabolism under different cardiac parameters. A mathematical model of EVHP combined with a virtual PID controller formed a closed-loop reference model to generate the reference trajectory of the MAP. The adaptive algorithm adjusted the control gain based on the reference state variable, the output variable, and the reference MAP. Simulations were performed to test the performance of the controller under varying heart conditions. Simulation results showed that the MRAC can tune control gains according to the changing cardiac parameters (e.g., resistance and compliance) and provide better transient performance than the conventional PID control. The experimental results demonstrated that the adaptive controller was able to achieve desired AoP levels and avoid overshoot when the MAP changed in large steps (e.g., 30-mmHg MAP change). Although the physiological responses of the six isolated hearts varied, the mean regulation error was consistently kept less than 2 mmHg. This brief, for the first time, proved that adaptive control can effectively regulate AoP of isolated pig hearts in an accurate (mean error less than 2 mmHg) and fast (4–8 s of settling time) manner. The future work is to evaluate this adaptive controller's effectiveness in the clinical setting.

References

[1] C. W. White *et al.*, "A cardioprotective preservation strategy employing *ex vivo* heart perfusion facilitates successful transplant of donor hearts after cardiocirculatory death," *J. Heart Lung Transplantation*, vol. 32, no. 7, pp. 734–743, Jul. 2013.

[2] L. Xin *et al.*, "A new multi-mode perfusion system for *ex vivo* heart perfusion study," *J. Med. Syst.*, vol. 42, no. 2, p. 25, Feb. 2018.

[3] L. Xin *et al.*, "Control of plants with input saturation nonlinearities," *ASAIO J.*, vol. 2019., pp. 1–10.

[4] C. W. White *et al.*, "A whole blood-based perfusate provides superior preservation of myocardial function during *ex vivo* heart perfusion," *J. Heart Lung Transplantation*, vol. 34, no. 1, pp. 21–113, 2015.

[5] T. Mayr *et al.*, "Large-animal biventricular working heart perfusion system with low priming volume–comparison between *in vivo* and *ex vivo* cardiac function," *Thoracic Cardiovascular Surgeon*, vol. 66, no. 1, pp. 71–82, Jan. 2018.

[6] P. Verdecchia, F. Angeli, R. Gattobigio, C. Rapicetta, and G. Reboldi, "Impact of blood pressure variability on cardiac and cerebrovascular complications in hypertension," *Amer. J. Hypertension*, vol. 20, no. 2, pp. 154–161, Feb. 2007.

[7] C. W. White *et al.*, "Avoidance of profound hypothermia during initial reperfusion improves the functional recovery of hearts donated after circulatory death," *Amer. J. Transplantation*, vol. 16, no. 3, pp. 773–782, Mar. 2016.

[8] A. van der Plaats, "The Groningen hypothermic liver perfusion system for improved preservation in organtransplantation," Dept. BioMed. Eng., Univ. Med. Center Groningen, Groningen, The Netherlands, Tech. Rep., 2005.

[9] I. C. J. H. Post, M. C. Dirkes, M. Heger, R. Bezemer, J. van't Leven, and T. M. van Gulik, "Optimal flow and pressure management in machine perfusion systems for organ preservation," *Ann. Biomed. Eng.*, vol. 40, no. 12, pp. 2698–2707, Dec. 2012.

[10] D. U. Campos-Delgado, I. Bonilla, M. Rodriguez-Martinez, M. E. Sanchez-Briones, and E. Ruiz-Hernandez, "Closed-loop control of renal perfusion pressure in physiological experiments," *IEEE Trans. Biomed. Eng.*, vol. 60, no. 7, pp. 1776–1784, Jul. 2013.

[11] J. A. Kornuta and J. Brandon Dixon, "Ex vivo lymphatic perfusion system for independently controlling pressure gradient and transmural pressure in isolated vessels," *Ann. Biomed. Eng.*, vol. 42, no. 8, pp. 1691–1704, Aug. 2014.

[12] N. Westerhof, J.-W. Lankhaar, and B. E. Westerhof, "The arterial Windkessel," *Med. Biol. Eng. Comput.*, vol. 47, no. 2, pp. 131–141, 2009.

[13] S. Maiti, C. Chakraborty, Y. Hori, and M. C. Ta, "Model reference adaptive controller-based rotor resistance and speed estimation techniques for vector controlled induction motor drive utilizing reactive power," *IEEE Trans. Ind. Electron.*, vol. 55, no. 2, pp. 594–601, 2008.

[14] Y. Yu, X. Sun, and W. Zhang, "Modeling and decoupling control for rotor system in magnetic levitation wind turbine," *IEEE Access*, vol. 5, pp. 15516–15528, 2017.

[15] E. H. Skorina, M. Luo, W. Tao, F. Chen, J. Fu, and C. D. Onal, "Adapting to flexibility: Model reference adaptive control of soft bending actuators," *IEEE Robot. Autom. Lett.*, vol. 2, no. 2, pp. 964–970, Apr. 2017.

[16] J. Brufau-Penella, K. Tsiakmakis, T. Laopoulos, and M. Puig-Vidal, "Model reference adaptive control for an ionic polymer metal composite in underwater applications," *Smart Mater. Struct.*, vol. 17, no. 4, Aug. 2008, Art. no. 045020.

[17] N. Beohar, V. N. K. Malladi, D. Mandal, S. Ozev, and B. Bakkaloglu, "Online built-in self-test of high switching frequency DC–DC converters using model reference based system identification techniques," *IEEE Trans. Circuits Syst. I, Reg. Papers*, vol. 65, no. 2, pp. 818–831, Feb. 2018.

[18] R. Khanna, Q. Zhang, W. E. Stanchina, G. F. Reed, and Z.-H. Mao, "Maximum power point tracking using model reference adaptive control," *IEEE Trans. Power Electron.*, vol. 29, no. 3, pp. 1490–1499, Mar. 2014.

[19] K.-H. Kim, "Model reference adaptive control-based adaptive current control scheme of a PM synchronous motor with an improved servo performance," *IET Electric Power Appl.*, vol. 3, no. 1, p. 8, 2009.

[20] R. Liao, B. K. Podesser, and C. C. Lim, "The continuing evolution of the langendorff and ejecting murine heart: New advances in cardiac phenotyping," *Amer. J. Physiol.-Heart Circulatory Physiol.*, vol. 303, no. 2, pp. H156–H167, Jul. 2012.

[21] J. Lee, D. E. Chambers, S. Akizuki, and J. M. Downey, "The role of vascular capacitance in the coronary arteries," *Circulat. Res.*, vol. 55, no. 6, pp. 751–762, 1984.

[22] A. J. Pappano and W. G. Wier, *Cardiovascular Physiology*, 10th ed. Philadelphia, PA, USA: Elsevier, 2013.

[23] G. Schillaci and G. Pucci, "The dynamic relationship between systolic and diastolic blood pressure: Yet another marker of vascular aging?" *Hypertension Res.*, vol. 33, no. 7, pp. 659–661, Jul. 2010.

[24] B. Gavish, I. Z. Ben-Dov, and M. Bursztyn, "Linear relationship between systolic and diastolic blood pressure monitored over 24h: Assessment and correlates," *J. Hypertension*, vol. 26, no. 2, pp. 199–209, Feb. 2008.

[25] N. Stergiopulos, B. E. Westerhof, and N. Westerhof, "Total arterial inertance as the fourth element of the Windkessel model," *Amer. J. Physiol.-Heart Circulatory Physiol.*, vol. 276, no. 1, pp. H81–H88, Jan. 1999.

[26] N. T. Nguyen, *Model-Reference Adaptive Control, in Model-Reference Adaptive Control: A Primer*. Cham, Switzerland: Springer, 2018, pp. 83–123.

[27] K. J. Åström and T. Hägglund, "Revisiting the Ziegler–Nichols step response method for PID control," *J. Process Control*, vol. 14, no. 6, pp. 635–650, Sep. 2004.

[28] H. Kaufman, I. Barkana, and K. Sobel, *Basic Theory of Simple Adaptive Control, in Direct Adaptive Control Algorithms: Theory and Applications*. New York, NY, USA: Springer, 1998, pp. 19–76.

[29] C. C. Palerm and B. W. Bequette, "Hemodynamic control using direct model reference adaptive control: Experimental results," *Eur. J. Control*, vol. 11, no. 6, pp. 558–571, Jan. 2005.

[30] H. Kaufman and G. W. Neat, "Asymptotically stable multiple-input multiple-output direct model reference adaptive controller for processes not necessarily satisfying a positive real constraint," *Int. J. Control*, vol. 58, no. 5, pp. 1011–1031, Nov. 1993.

[31] I. D. Landau, "A survey of model reference adaptive techniques—Theory and applications," *Automatica*, vol. 10, no. 4, pp. 353–379, 1974.

[32] J. C. Doyle, R. S. Smith, and D. F. Enns, "Control of plants with input saturation nonlinearities," in *Proc. Amer. Control Conf.*, 1987, pp. 1034–1039.